FEBS Letters 581 (2007) 3247–3252

Carnitine palmitoyltransferase 2: Analysis of membrane association and complex structure with a substrate analog

Arne C. Rufer[a,1], Andrei Lomize[b], Jörg Benz[a], Odile Chomienne[a], Ralf Thoma[a], Michael Hennig[a,*]

[a] *F. Hoffmann-La Roche AG, Pharma Research Discovery, 4070 Basel, Switzerland*
[b] *College of Pharmacy, University of Michigan, Ann Arbor, Michigan 48109-1065, USA*

Received 20 March 2007; revised 29 May 2007; accepted 30 May 2007

Available online 8 June 2007

Edited by Stuart Ferguson

Abstract The mitochondrial membrane-associated carnitine palmitoyltransferase system is a validated target for the treatment of type 2 diabetes mellitus. To further facilitate structure-based drug discovery, we determined the crystal structure of rat CPT-2 (rCPT-2) in complex with the substrate analogue palmitoyl-aminocarnitine at 1.8 Å resolution. Biochemical analyses revealed a strong effect of this compound on rCPT-2 activity and stability. Using a computational approach we examined the membrane association of rCPT-2. The protein interacts with the membrane as a functional monomer and the calculations confirm the presence of a membrane association domain that consists of layers of hydrophobic and positively charged residues.

Keywords: Type 2 diabetes mellitus; Drug discovery; Membrane protein

1. Introduction

Cytosolic long-chain fatty acid (LCFA)-CoA esters are transported into mitochondria by two carnitine acyltransferase (CPT) enzymes in conjunction with a carnitine/acylcarnitine translocase (CACT) [1]. CPT-1 is an integral membrane protein of the outer mitochondrial membrane and catalyzes the transesterification of LCFA-CoA to acylcarnitine, which is transferred into the mitochondrial lumen by CACT. CPT-2 converts acylcarnitine back to LCFA-CoA, thereby providing substrates for β-oxidation.

Pharmacological attenuation of mitochondrial LCFA import by inhibition of CPT-1 has been shown to ameliorate the symptoms of diverse diseases such as type 2 diabetes mellitus (T2D), psoriasis and myocardial infarction in animal models [2–5]. Modulation of CPT-1 activity has also been implicated in prevention of cardiac reperfusion injury [6], pancreatic insulin secretion [7], sepsis [8] and apoptosis [9].

The most advanced medicinal chemistry programs focus on inhibitors of the CPT system in liver as a target for the treatment of T2D. While chemically diverse CPT inhibitors have been described [10], the class of non-hydrolyzable acylaminocarnitine analogs of the CPT-1 product acylcarnitine are the best characterized [2,3,11–14]. Recently, we reported the crystal structure of rat CPT-2 (rCPT-2) in complex with ST1326 [15], which is an ureido-acylaminocarnitine. A derivative of this inhibitor class, (*S*)-*N*-palmitoylated aminocarnitine (compound 16 of the series described in [3]), is also a potent CPT-directed inhibitor of mitochondrial LCFA import.

Here we report the elucidation of the binding mode of compound 16 in complex with rCPT-2 by crystal structure analysis at 1.8 Å resolution. Compound 16 more closely resembles the physiological CPT-2 substrate palmitoyl-carnitine (only the ester oxygen is exchanged against nitrogen) when compared to ST1326. Improved resolution and data quality compared to the rCPT-2 · ST1326 complex now allows for an accurate superimposition of inhibited and uninhibited molecular structures of rCPT-2. Titration of rCPT-2 with compound 16 in a fluorescence-based thermal shift assay revealed a pronounced concentration dependent effect on the stability of the complex. Analysis of the rCPT-2 structure with a novel computational approach [16,17] substantiates that a previously identified rCPT-2-specific sequence insertion [15,18] serves as membrane anchor.

2. Materials and methods

Cloning, purification and the activity assay of His_6-tagged rCPT-2 were performed as described [15]. Crystallization and the thermal shift assay described herein were performed with rCPT-2 in a buffer containing 25 mM Tris/HCl (pH 8), 0.15 M NaCl, 2 mM tris(2-carboxyethyl)phosphine (TCEP) as reducing agent, 1% (w/v) β-octylglucoside (βOG) and 0.02% (w/v) NaN_3. Compound 16 [R-3-(hexadecanoylamino)-4-(trimethylazaniumyl)butanoate] was synthesized in-house according to Shinagawa et al. [3].

2.1. Thermal shift assay

The experimental design was adapted from a published fluorescence-based thermal shift assay [19]. rCPT-2 (1 μM) was pre-incubated with the fluorescence probe Sypro Orange (Molecular Probes) and compound 16. The fluorescence signal was recorded on a Bio-Rad MyiQ real-time PCR machine with an excitation wavelength of 490 nm and an emission wavelength of 530 nm (the absorption and emission maxima of Sypro Orange are 470 nm and 570 nm, respectively) and

*Corresponding author. Fax: +41 61 6887408.
E-mail address: michael.hennig@roche.com (M. Hennig).

[1]Present address: Max-Planck-Institute for Medical Research, Department of Biomolecular Mechanisms, 69120 Heidelberg, Germany.

Abbreviations: βOG, β-octylglucoside; CACT, carnitine/acylcarnitine translocase; CPT, carnitine palmitoyltransferase; LCFA, long-chain fatty acid; T2D, type 2 diabetes mellitus

0014-5793/$32.00
doi:10.1016/j.febslet.2007.05.080

a heating rate of 1 °C/min. The fluorescence signal was corrected for baseline drift due to thermal disintegration and photo bleaching of the fluorescence probe. The melting points of rCPT-2 were obtained by fitting first derivative plots of the fluorescence data produced with Bio-Rad software to the first derivative of the equation described by Pantoliano et al. [19]:

$$\frac{\partial F}{\partial T} = -\frac{\exp\left[-\frac{\Delta H_{un}\left(\frac{1}{T}-\frac{1}{T_m}\right)}{R}+\frac{\Delta C_{p,un}\left(-1+\frac{T_m}{T}+\ln\frac{T}{T_m}\right)}{R}\right](F_N-F_U)\left[\frac{\Delta H_{un}}{RT^2}+\frac{\Delta C_{p,un}\left(\frac{1}{T}-\frac{T_m}{T^2}\right)}{R}\right]}{\left[1+\exp\left(-\frac{\Delta H_{un}\left(\frac{1}{T}-\frac{1}{T_m}\right)}{R}+\frac{\Delta C_{p,un}\left(-1+\frac{T_m}{T}+\ln\frac{T}{T_m}\right)}{R}\right)\right]^2} \quad (1)$$

where F is the fluorescence dependent on temperature T, F_N and F_U are the fluorescence prior to (native state) and after (unfolded state) the thermal melting process, T_m is the melting point, ΔH_{un} and $\Delta C_{p,un}$ are the enthalpy of protein unfolding and the change in protein heat capacity during unfolding in the absence of ligand and R is the gas constant. See supplementary Fig. 1 for fits.

2.2. Protein crystallization

rCPT-2 at 12–18 mg/ml was incubated with a 10-fold molar excess of compound 16 and subsequently co-crystallized by vapor diffusion with 0.15 M DL-malic acid pH 7.0, 20% (w/v) PEG 3350 (Index 91, Hampton Research). Micro-seeds of unliganded rCPT-2 crystals were added prior to drop setup. Crystals were flash frozen in liquid nitrogen after exchanging excess mother liquor and Al's oil against 100% (v/v) paraffin oil.

2.3. Data collection and processing

A dataset for the rCPT-2 · compound 16 complex was collected from a single crystal at 100 K with $\lambda = 0.9795$ Å on beam line X10SA at SLS, Villigen, Switzerland, processed and scaled with XDS [20]. Data statistics are summarized in Table 1.

2.4. Structure solution and refinement

Molecular replacement was performed with the program Phaser [21] using structure of PDB entry 2DEB [15] as search model. The final model at 1.78 Å resolution was built using cycles of model building in MOLOC [22] solvent building in autoBUSTER [23] and refinement in Refmac [24]. For the final structure 93.4% of the residues lie in the most favored, 6.2% in the additionally allowed regions and Leu 129 as well as Asn 230 are outliers of the Ramachandran plot. Refinement statistics are summarized in Table 1. CNS [25] was used for calculating simulated annealing omit maps (1000 K starting temperature). Structure figures were prepared with PyMOL [26].

2.5. Calculation of rCPT-2 membrane interaction

Unlike transmembrane proteins, peripheral proteins do not span the membrane. Therefore, they have no hydrophobic thickness, and their $\Delta G_{transfer}$ depends on only three variables (D, τ and φ). Instead of the hydrophobic thickness, we calculated the maximal membrane penetration depths (D) for the membrane anchor of monotopic membrane proteins. The tilt angle (τ, and its directionality φ) of peripheral proteins was calculated as the angle between the bilayer normal and the long molecular axis of the protein. The latter was defined as an axis providing the minimal moment of inertia of the protein [27].

This computational approach for positioning of proteins in membranes has been previously developed and tested for 109 transmembrane and 476 peripheral or integral monotopic membrane proteins [16,17,28]. A protein is considered a rigid body that freely floats in the fluid hydrocarbon core of a lipid bilayer. Free energy of the protein was represented as sum of transfer energies of all its atoms from water to the hydrocarbon core of the lipid bialyer ($\Delta G_{transfer}$) and ionization energies of charged residues (ΔG_{pK}). The energy was optimized in a coordinate system whose Z axis coincided with the bilayer normal. It depends on only three variables (φ, τ, D):

$$\Delta G_{calc}(\varphi,\tau,D) = \Delta G_{transfer} + \Delta G_{pK} \quad (2)$$

where D is a shift of the protein center along the Z axis, τ is a tilt angle of longitudinal protein axis relative to the Z axis (membrane normal), φ is a rotation angle that defines the direction of the tilt.

Transfer energy of a protein was calculated using the implicit solvation model:

$$\Delta G_{transfer} = \sum_i \mathrm{ASA}_i \sigma_i^{W-M} f(z_i) \quad (3)$$

where ASA_i is the accessible surface area of atom i, and σ_i^{W-M} is the solvation parameter of atom i (its transfer energy from water to membrane interior expressed in kcal/mol per Å^2). ASA were determined using the subroutine SOLVA from NACCESS (kindly provided by Hubbard and Thornton, Department of Biochemistry and Molecular Biology, University College London) with radii of Chothia [29], without hydrogen atoms, and with a probe radius of 1.4 A.

All atomic solvation parameters were previously derived from the partition coefficients of organic compounds between water and decadiene [30]. These parameters are normalized by the effective concentration of water, which changes gradually in a narrow region between the lipid head group region and the hydrocarbon core. We used a sigmoidal water concentration profile, as determined in EPR studies on spin-labeled phospholipids [31]:

$$f(z_i) = 1/(1+e^{(|z_i|-z_0)/\lambda}) \quad (4)$$

Table 1
Data collection and refinement statistics

Data collection	Compound 16
Space group	$C222_1$
Cell dimensions	
a, b, c (Å)	95.3, 97.8, 312.1
Matthews' coefficient (2 mol/AU)	2.5
Resolution (Å)[a]	50.0 −1.78 (1.89–1.78)
R_{sym}[b]	3.4 (7.8)
$I/\sigma I$	22.26 (12.71)
Completeness (%)	95.6 (91.0)
Redundancy	7.2 (6.4)
Refinement	
Resolution (Å)	50.0–1.78
No. reflections	120296 (8937, working set)
R_{work}/R_{free}[c]	17.7 (19.6)/22.3 (28.9)
No. atoms	11167
Protein	10085
Ligand	56 [20][d]
Water	1076
B-factors (overall)	18.3
Protein	17.6
Ligand	18.9 [55.1][d]
Water	24.3
R.m.s. deviations	
Bond lengths (Å)	0.012
Bond angles (°)	1.278

[a]Values in parentheses are for the highest resolution shell (1.781–1.827 Å).
[b]$R_{sym} = \sum|I(h)_j - \langle I(h)\rangle|/\sum I(h)j$.
[c]$R = \sum||F_{obs}| - |F_{calc}||/\sum|F_{obs}|$, R_{free} was calculated using a randomly selected set (5%) of reflections.
[d]Compound 16. B-factor of single βOG attached to molecule A in brackets.

The characteristic distance λ of this profile was chosen as 0.9 Å. All charged residues of the protein were considered neutral in the membrane hydrocarbon core. The corresponding ionization energy was described by the Henderson–Hasselbalch equation, where the ionization energy of each residue k is distributed between its charged side-chain O or N atoms proportional to their relative accessible surface areas ASA_i:

$$\Delta G_{pK} = 2.3RT \sum_{k=1}^{N} \left[(pH - pK_k) \sum_{i=1}^{M_i} (ASA_i / ASA_k^{tot}) f(z_i) \right] \quad (5)$$

where ASA_k^{tot} is total ASA of all charged atoms in this residue, and pK values of Asp, Glu, Lys and Arg residues are chosen as described previously [16] the penalty for His is zero, since it is uncharged at pH 7. Global energy minimization was performed by combining a grid scan and the Davidon–Fletcher–Powell method [16]. Heteroatoms were not included in the calculations.

3. Results and discussion

3.1. Overall structure and compound 16 binding mode

The overall fold and positions Cα atoms of the present and previously reported rCPT-2 structures are essentially identical with a root-mean-square-deviation (RMSD) of 0.23–0.47 Å (Table 2). Compound 16 is located in a large tunnel that penetrates rCPT-2. The hydrophilic head-group of the molecule binds to the centre of that tunnel with direct hydrogen-bonds to the side-chains of residues Tyr120, His372, Ser488, Thr499 and Ser590 (Fig. 1A and B). The C15-alkyl part of the ligand occupies the essentially hydrophobic tunnel from the centre of the molecule to the surface. While the overall topology of rCPT-2 is retained in the inhibited and uninhibited states of the enzyme, the superimposition of these two states emphasizes a rearrangement of active site residues occurring upon ligand binding (Fig. 1A and B). The electron density of the side-chain of Tyr120 is better defined in the structures with bound inhibitor as compared to uninhibited rCPT-2 (data not shown) and indicates that the hydroxyl oxygen of Tyr120 moves approximately 4 Å towards the ligand binding site. This movement establishes the hydrogen bonding network also involving residues Asp376 and Arg498, which is important for the alignment of a conserved water molecule and proper substrate binding in the active site [15]. The entire catalytic loop of rCPT-2 spanning residues His372–Gly377 undergoes a change in conformation upon binding of compound 16 in order to position Asp376 in the hydrogen network. The ability of the catalytic loop to adopt different conformations is emphasized by a peptide-plane flip between residues Asp376 and Gly377 in the compound 16 complex structure (Fig. 1B). No correlation exists between the orientation of the peptide-plane and presence of the aminocarnitine inhibitors since the peptide-flip occurs neither in the ST1326 complex or uninhibited structures nor in the rCPT-2 structure solved by Hsiao et al. [18]. Compound 16 and ST1326 are nearly isosteric with regard to ligand structure but the peptide-flip induces differences in the ligand pockets of rCPT-2 in the complex structures. The distance from the carbonyl-oxygen of the Asp376–Gly377 peptide bond to the acylic β carbon atom of compound 16 is 6.3 Å (6.27 Å) in chain A (chain B), whereas the equivalent distance to the linker nitrogen of ST1326 is 5.04 Å. Gly377 immediately precedes helix α17 (residues Val378–Thr394) of rCPT-2. The carbonyl-oxygen of the Asp376–Gly377 peptide bond in the compound 16 complex is situated within hydrogen bonding distance (2.99 Å and 3.14 Å for chain A and B) to the amino-nitrogen atoms of Val378, Ala379 and Val380.

Table 2
Pairwise RMSD of rCPT-2 structure superimpositions[a]

Superimposition	RMSD (Å)
rCPT-2 · compound 16 (chain A)[b] – compound 16 (chain B)	0.26
rCPT-2 · compound 16 (chain A) – 2DEB[c] (chain A, uninhibited)	0.23
rCPT-2 · compound 16 (chain A) – 2FW3[d] (ST1316)	0.42
rCPT-2 · compound 16 (chain B) – 2FW3 (ST1316)	0.46

[a]RMSD for rCPT-2 · compound 16-2H4T (P1) [18] = 0.43–0.47 Å.
[b]$C222_1$.
[c]$C222_1$.
[d]$P2_12_12_1$.

Important questions raised by these observations are under which conditions the peptide-flip is energetically favored and whether this peptide-flip can also occur in L-CPT-1. Interestingly, the average *B*-factor of all catalytic loop atoms is 13.2 $Å^2$ (chain A), which is significantly lower than the average *B*-factor of the entire protein and is also true for the uninhibited state of rCPT-2. This implies that the observed features are likely due to two discrete conformations and not a result of high loop flexibility. The presence of a conserved proline residue could render the catalytic loop of CPT-1 isoforms less flexible than that of CPT-2. Bridging the approximately 5 Å gap between the scaffold of the established aminocarnitine compounds and the Asp376–Gly377 is feasible for a medicinal chemistry program and, therefore, this peptide bond could provide a novel anchor point for isoform-specific CPT inhibitors.

3.2. Compound 16 complex and implications for protein stability

Compound 16 inhibits rCPT-2 with an IC_{50} of 210 ± 34 nM (Fig. 1C) as determined with our activity assay which is similar to the inhibition observed in the presence of ST1326 (IC_{50} = 240 nM) [15]. This implies that the link between the aminocarnitine head-group and the acyl-moiety can be subject to chemical optimization in order to improve, e.g., chemical tractability, stability and physico-chemical properties.

The fluorescence-based thermal shift assay produced a melting point (T_m) of 47.6 ± 0.1 °C for uninhibited rCPT-2 (Fig. 1D, supplementary figure 1). This value is in good agreement with the T_m of 47.0 ± 0.5°C determined with circular dichroism (data not shown). The T_m is elevated in a concentration dependent manner in the presence of compound 16, which stabilizes rCPT-2 with a half-maximal effective concentration of 190 ± 91 nM. A threefold molar excess of compound 16 leads to an increase in the melting point by approximately 10 °C. This pronounced effect on the stability of rCPT-2 can be attributed to improved interactions between the amino- and carboxy-terminal domains as well as stabilization and extension of the hydrophobic core of rCPT-2 due to binding of compound 16 at the domain interface (Fig. 1A). In rCPT-2 β-strands 1 and 16 constitute the major domain contact and line the hydrophobic acyl-tunnel that accommodates the alkyl moiety of compound 16. The results of the thermal shift assay corroborate those of the activity assay in demonstrating that compound 16 is a high-affinity inhibitor of rCPT-2 in vitro and that these assays can be used for the examination of ligand binding to detergent-solubilized rCPT-2. However, the effect of

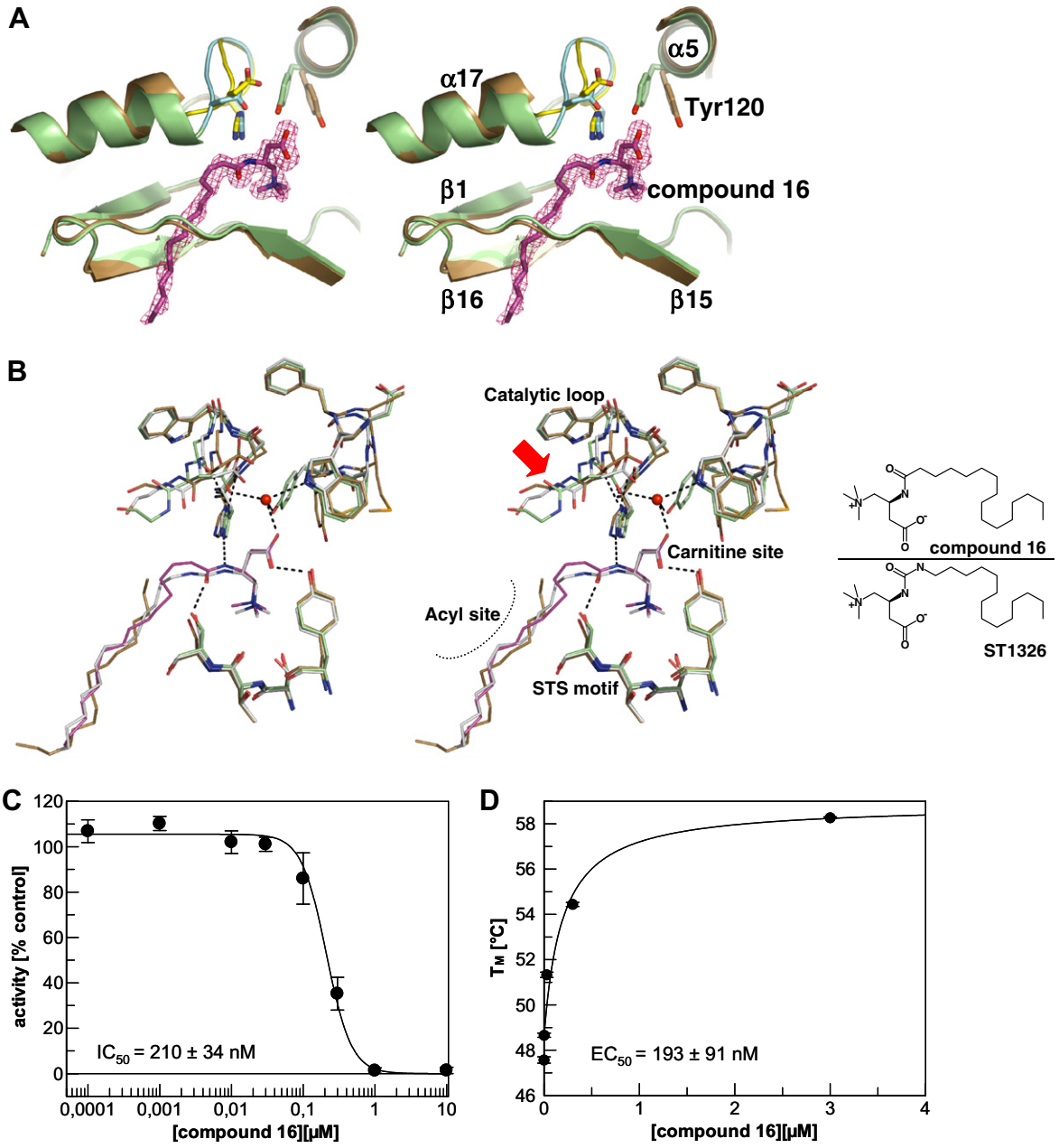

Fig. 1. Binding of compound 16 to rCPT-2: (A) stereo-diagram of the superimposition of the rCPT-2 · compound 16 complex (green, residues His372 to Gly377 of catalytic loop in cyan) and uninhibited rCPT-2 (brown, catalytic loop in yellow; PDB code 2DEB) is shown. Residues Tyr120, Asp 376, and the catalytic His372 are displayed as stick models. Compound 16 (magenta) is shown with its surrounding F_o–F_c-simulated annealing omit electron density map (pink) contoured at 3σ. (B) Stereo-view of the peptide-plane flip (red arrow) between Asp376 and Gly377 of the catalytic loop. The compound 16 complex (green; hydrogen-bonds are depicted as dashed black lines), the ST1326 complex (gray) and the uninhibited structure (brown, with its fortuitous C16 ligand) are shown. The conserved water molecule of the complex structures is shown as red sphere. The structure of compound 16 is compared to those of ST1326 and palmitoyl-carnitine in the right panel. (C) Inhibition of 30 nM rCPT-2 by compound 16. The data were fitted using a 3 parameter equation describing a background corrected dose–response curve. (D) Increase of T_m caused by binding of compound 16 to 1 μM rCPT-2. Data in panels C and D were processed with GraFit (Erithacus Software Ltd.), means ± S.D. of three (two) independent experiments are shown, respectively.

the detergent, βOG, on the activity of CPT-2 [32,33] and on the partition of compound 16 into detergent micelles remains debatable and further studies for example by isothermal calorimetry are desirable to resolve this uncertainty.

3.3. Membrane association of rCPT-2

The role of the sequence insertion comprising residues Asn179–Asn208 as membrane anchor [15,18] could be further established by means of a computational method [16]. For the complex of rCPT-2 and compound 16 we calculated a maximal membrane penetration depth of 4.5 ± 1.0 Å, a tilt angle of 69 ± 6° and $\Delta G_{transfer}$ of −8.2 kcal/mol (Fig. 2). Similar values could be calculated for rCPT-2 in its uninhibited form and for the complex with ST1326 (data not shown). Besides limitations in the assumptions made for the algorithm, the calculated orientations of different rCPT-2 structures are slightly affected by

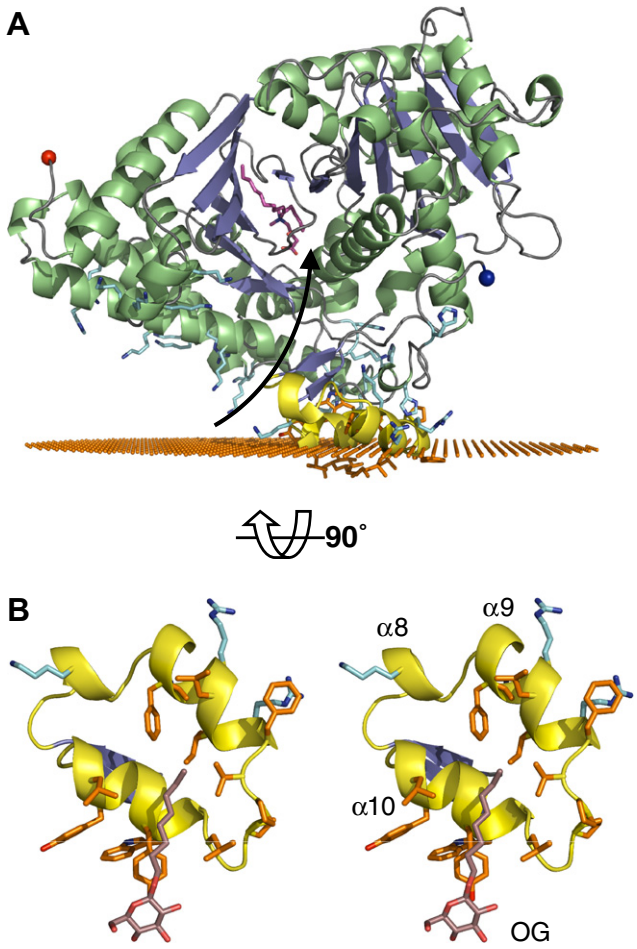

Fig. 2. Membrane association of rCPT-2: (A) α-helices, β-sheets and loops are depicted as green, blue and gray cartoon, respectively. The insert (yellow, hydrophobic residues are shown as orange stick models) is proposed to submerge into the hydrophobic core of the luminal aspect of the inner mitochondrial membrane, which is indicated by orange spheres. A single βOG molecule bound to the insert is shown as light-brown stick model. The amino- and carboxy-termini are indicated with blue and red spheres, respectively. Basic residues important for membrane association are shown as cyan stick models. The arrow traces the proposed entrance of the substrate palmitoyl-carnitine into the catalytic site via the transporter CACT [15]. (B) same as A but in stereo view and rotated 90° to the back so that the planes of the membrane and the figure coincide. Only the insert comprising α-helices 8–10 with the adjacent β-strands 2 and 3 are shown.

conformers of flexible side-chains at the protein surface and, therefore, could potentially be biased by crystal packing and resolution of the X-ray structures. Nevertheless, the results of our calculations support the notion that rCPT-2 interacts with the mitochondrial membrane as a monomer. We observed loosely packed dimers of rCPT-2 in crystal structures with space group $C222_1$. However, the exposed non-polar regions of two molecules do not form a continuous surface at one side of the dimer, as would be expected for a functional self-associated state of rCPT-2. The calculated position of the inner mitochondrial membrane as shown in Fig. 2 coincides very well with a layer of hydrophobic residues of the membrane association domain. In this model hydrophobic residues such as Phe188, Phe194, Leu191, Leu199, Leu206, Pro196 and Val207 would submerge into the core of the membrane. Electron density indicating specific binding of a βOG molecule to the insert supports this interpretation. A layer of positively charged residues from the insert (Lys182, Arg190, Arg193) would facilitate association with the polar hydrophilic head-groups of cardiolipin molecules of the inner mitochondrial membrane [15]. This layer of basic amino acids is extended further at the core of the protein molecule by Lys56, Lys104, Lys107, Lys534, Lys537, Lys544 and several more residues. From the calculated membrane model no direct contact of these latter residues to polar groups of the membrane can be inferred (Fig. 2A). However, the model assumes a planar geometry for the membrane and does not take into account membrane curvature [34]. A curved membrane would enable a tight contact with the protein surface supporting the proposed path of the substrate palmitoyl-carnitine from the membrane, potentially facilitated by the transporter CACT, into the catalytic site of the enzyme. This mode of substrate channeling into rCPT-2 would be in line with the intriguing concept of mitochondrial microcompartmentation proposed by Murthy and Pande [35].

In summary, the structure of rCPT-2 in complex with compound 16 provides further insight into the ligand binding mode and conformational flexibility of rCPT-2 that could be used in the design of novel selective CPT inhibitors. The analysis of the membrane binding by computational tools confirms the hypothesis of a membrane association domain and provides an indication of the localization of inner the mitochondrial membrane with respect to rCPT-2, which is important for the understanding of the acylcarnitine transport through the membrane.

Acknowledgements: The authors acknowledge L. Hilfiger and C. Karrer for technical assistance with activity assays, B. Gsell with purification and M. Stihle with crystallization. The staff members at SLS, Villigen, Switzerland are acknowledged for support with data collection.

Appendix A. Supplementary data

Supplementary data associated with this article can be found, in the online version, at doi:10.1016/j.febslet.2007.05.080.

References

[1] McGarry, J.D. and Brown, N.F. (1997) The mitochondrial carnitine palmitoyltransferase system. From concept to molecular analysis. Eur. J. Biochem. 244, 1–14.
[2] Kanamaru, T., Shinagawa, S., Asai, M., Okazaki, H., Sugiyama, Y., Fujita, T., Iwatsuka, H. and Yoneda, M. (1985) Emeriamine, an antidiabetic beta-aminobetaine derived from a novel fungal metabolite. Life Sci. 37, 217–223.
[3] Shinagawa, S., Kanamaru, T., Harada, S., Asai, M. and Okazaki, H. (1987) Chemistry and inhibitory activity of long chain fatty acid oxidation of emeriamine and its analogues. J. Med. Chem. 30, 1458–1463.
[4] Caspary, F., Elliott, G., Navé, B.T., Verzaal, P., Rohrbach, M., Das, P.K., Nagelkerken, L. and Nieland, J.D. (2005) A new therapeutic approach to treat psoriasis by inhibition of fatty acid oxidation by Etomoxir. Br. J. Dermatol. 153, 937–944.
[5] Grynberg, A. (2005) Effectors of fatty acid oxidation reduction: promising new anti-ischaemic agents. Curr. Pharm. Des. 11, 489–509.
[6] Lopaschuk, G.D., Wall, S.R., Olley, P.M. and Davies, N.J. (1988) Etomoxir, a carnitine palmitoyltransferase I inhibitor, protects

hearts from fatty acid-induced ischemic injury independent of changes in long chain acylcarnitine. Circ. Res. 63, 1036–1043.
[7] Lehtihet, M., Welsh, N., Berggren, P.O., Cook, G.A. and Sjoholm, A. (2003) Glibenclamide inhibits islet carnitine palmitoyltransferase 1 activity, leading to PKC-dependent insulin exocytosis. Am. J. Physiol. Endocrinol. Metab. 285, E438–E446.
[8] Eaton, S., Fukumoto, K., Stefanutti, G., Spitz, L., Zammit, V.A. and Pierro, A. (2003) Myocardial carnitine palmitoyltransferase I as a target for oxidative modification in inflammation and sepsis. Biochem. Soc. Trans. 31, 1133–1136.
[9] Mutomba, M.C., Yuan, H., Konyavko, M., Adachi, S., Yokoyama, C.B., Esser, V., McGarry, J.D., Babior, B.M. and Gottlieb, R.A. (2000) Regulation of the activity of caspases by L-carnitine and palmitoylcarnitine. FEBS Lett. 478, 19–25.
[10] Anderson, R.C. (1998) Carnitine palmitoyltransferase: a viable target for the treatment of NIDDM? Curr. Pharm. Des. 4, 1–16.
[11] Jenkins, D.L. and Griffith, O.W. (1985) DL-Aminocarnitine and acetyl-DL-aminocarnitine. Potent inhibitors of carnitine acyltransferases and hepatic triglyceride catabolism. J. Biol. Chem. 260, 14748–14755.
[12] Jenkins, D.L. and Griffith, O.W. (1986) Antiketogenic and hypoglycemic effects of aminocarnitine and acylaminocarnitines. Proc. Natl. Acad. Sci. USA 83, 290–294.
[13] Giannessi, F., Chiodi, P., Marzi, M., Minetti, P., Pessotto, P., De Angelis, F., Tassoni, E., Conti, R., Giorgi, F., Mabilia, M., Dell'Uomo, N., Muck, S., Tinti, M.O., Carminati, P. and Arduini, A. (2001) Reversible carnitine palmitoyltransferase inhibitors with broad chemical diversity as potential antidiabetic agents. J. Med. Chem. 44, 2383–2386.
[14] Giannessi, F., Pessotto, P., Tassoni, E., Chiodi, P., Conti, R., De Angelis, F., Dell'Uomo, N., Catini, R., Deias, R., Tinti, M.O., Carminati, P. and Arduini, A. (2003) Discovery of a long-chain carbamoyl aminocarnitine derivative, a reversible carnitine palmitoyltransferase inhibitor with antiketotic and antidiabetic activity. J. Med. Chem. 46, 303–309.
[15] Rufer, A.C., Thoma, R., Benz, J., Stihle, M., Gsell, B., De Roo, E., Banner, D.W., Mueller, F., Chomienne, O. and Hennig, M. (2006) The crystal structure of carnitine palmitoyltransferase 2 and implications for diabetes treatment. Structure 14, 713–723.
[16] Lomize, A.L., Pogozheva, I.D., Lomize, M.A. and Mosberg, H.I. (2006) Positioning of proteins in membranes: a computational approach. Protein Sci. 15, 1318–1333.
[17] Lomize, M.A., Lomize, A.L., Pogozheva, I.D. and Mosberg, H.I. (2006) OPM: orientations of proteins in membranes database. Bioinformatics 22, 623–625.
[18] Hsiao, Y.S., Jogl, G., Esser, V. and Tong, L. (2006) Crystal structure of rat carnitine palmitoyltransferase II (CPT-II). Biochem. Biophys. Res. Commun. 346, 974–980.
[19] Pantoliano, M.W., Petrella, E.C., Kwasnoski, J.D., Lobanov, V.S., Myslik, J., Graf, E., Carver, T., Asel, E., Springer, B.A., Lane, F.R. and Salemme, F.R. (2001) High-density miniaturized thermal shift assays as a general strategy for drug discovery. J. Biomol. Screen. 6, 429–440.
[20] Kabsch, W. (1992) Automatic processing of rotation diffraction data from crystals of initially unknown symmetry and cell constants. J. Appl. Cryst. 26, 795–800.
[21] McCoy, A.J., Grosse-Kunstleve, R.W., Storoni, L.C. and Read, R.J. (2005) Likelihood-enhanced fast translation functions. Acta Crystallogr. D Biol. Crystallogr. 61, 458–464.
[22] Gerber, P.R. (1992) Peptidemechanics: a force field for peptides and proteins working with entire residues as small units. Biopolymers 32, 1003–1017.
[23] Roversi, P., Blanc, E., Vonrhein, C., Evans, G. and Bricogne, G. (2000) Modelling prior distributions of atoms for macromolecular refinement and completion. Acta Crystallogr., D Biol. Crystallogr. 56, 1316–1323.
[24] Murshudov, G.N., Vagin, A.A., Lebedev, A., Wilson, K.S. and Dodson, E.J. (1999) Efficient anisotropic refinement of macromolecular structures using FFT. Acta Crystallogr., D Biol. Crystallogr. 55, 247–255.
[25] Brünger, A.T. (1992) X-PLOR Manual Version 3.1, Yale University Press, New Haven, CT, USA.
[26] DeLano, W.L. (2002) The PyMOL User's Manual, DeLano Scientific, San Carlos.
[27] Brunecky, R., Lee, S., Rzepecki, P.W., Overduin, M., Prestwich, G.D., Kutateladze, A.G. and Kutateladze, T.G. (2005) Investigation of the binding geometry of a peripheral membrane protein. Biochemistry 44, 16064–16071.
[28] Lomize, A.L., Pogozheva, I.D., Lomize, M.A. and Mosberg, H.I. Key role of hydrophobic interactions for positioning of peripheral proteins in membranes, personal communication.
[29] Chothia, C. (1975) Structural invariants in protein folding. Nature 254, 304–308.
[30] Lomize, A.L., Pogozheva, I.D. and Mosberg, H.I. (2004) Quantification of helix–helix binding affinities in micelles and lipid bilayers. Protein Sci. 13, 2600–2612.
[31] Marsh, D. (2002) Membrane water-penetration profiles from spin labels. Eur. Biophys. J. 31, 559–562.
[32] Fiol, C.J. and Bieber, L.L. (1988) Effects of octylglucoside and triton X-100 on the kinetics and specificity of carnitine palmitoyltransferase. Lipids 23, 120–125.
[33] Ramsay, R.R., Gandour, R.D. and van der Leij, F.R. (2001) Molecular enzymology of carnitine transfer and transport. Biochim. Biophys. Acta 1546, 21–43.
[34] Zimmerberg, J. and Kozlov, M.M. (2006) How proteins produce cellular membrane curvature. Nat. Rev. Mol. Cell. Biol. 7, 9–19.
[35] Murthy, M.S. and Pande, S.V. (1984) Mechanism of carnitine acylcarnitine translocase-catalyzed import of acylcarnitines into mitochondria. J. Biol. Chem. 259, 9082–9089.